

# Improving the image quality of short-time bone SPECT using cadmium-zinc-telluride detectors with SwiftScan

Kazuto Funakoshi<sup>1\*</sup>, Tomohiko Yamane<sup>2,3</sup>, Eito Kozawa<sup>4</sup>, Ichiro Matsunari<sup>5</sup>

<sup>1</sup>Department of Radiation Oncology, Saitama Medical University Hospital, Saitama, Japan

<sup>2</sup>Department of Molecular Imaging Research, Kobe City Medical Center General Hospital, Hyogo, Japan

<sup>3</sup>Department of Nuclear Medicine, International Medical Center, Saitama Medical University, Saitama, Japan

<sup>4</sup>Department of Radiology, Saitama Medical University Hospital, Saitama, Japan

<sup>5</sup>Department of Nuclear Medicine, Saitama Medical University Hospital, Saitama, Japan

## ARTICLE INFO

Article type:

Original Article

Article history:

Received: 21 Dec 2023

Revised: 24 Jul 2024

Accepted: 16 Aug 2024

Keywords:

Short-time bone SPECT/CT

CZT semiconductor camera

SwiftScan

## ABSTRACT

**Objective(s):** This study aimed to evaluate the quality and associated quantitative values of bone single-photon emission computed tomography (SPECT) with and without SwiftScan using a semiconductor camera equipped with a cadmium-zinc-telluride detector.

**Methods:** Ten patients with bone metastases from prostate cancer who underwent list-mode SPECT/computed tomography using a whole-body semiconductor camera participated in this study. A total of 130 metastatic lesions from 10 patients were analyzed. Standard SPECT images were obtained approximately 3 h later, and the images were constructed with and without SwiftScan.

**Results:** The visual assessment of 3-dimensional maximum intensity projection images showed that when an image quality score of 4 (good) or better was considered clinically acceptable, it was maintained at 4 or better in the 75% and 50% scans with SwiftScan, whereas only the 75% scan was considered acceptable without SwiftScan. The intraclass correlation coefficient was 0.952 at 5% for the standard time without SwiftScan and 0.990 with SwiftScan. The maximum standardized uptake value (SUV<sub>max</sub>) changes were 0 to 9.5 (median 1.1) at 75%, 0.1 to 11.5 (1.65) at 50%, 0 to 15.7 (2.1) at 25%, 0.1 to 33.2 (4.2) at 10%, 0.2 to 8.9 (5.65) at 5% without SwiftScan. On the contrary, the SUV<sub>max</sub> changes in absolute value were 0 to 5.4 (median 0.8) at 75%, 0 to 6.5 (1.4) at 50%, 0 to 19.1 (1.7) at 25%, 0 to 24.2 (2.8) at 10%, 0 to 29.9 (2.6) at 5% with SwiftScan. The contrast-to-noise ratios (CNR) were 95.3 at 75%, 88.3 at 50%, 69.2 at 25%, 45.7 at 10%, and 31.6 at 5% without SwiftScan, and 96.9, 91.7, 78.0, 71.6, and 62.0, respectively, using SwiftScan.

**Conclusion:** With the use of SwiftScan, a 50% reduction in acquisition time was considered acceptable for image quality with reproducible quantitative indices such as SUV<sub>max</sub> and CNR.

► Please cite this paper as:

Funakoshi K, Yamane T, Kozawa E, Matsunari I. Improving the image quality of short-time bone SPECT using cadmium-zinc-telluride detectors with SwiftScan. Asia Ocean J Nucl Med Biol. 2025; 13(1): 87-93. doi: 10.22038/aojnmb.2024.76919.1543

## Introduction

Patients with localized prostate cancer have a 5-year survival rate of >99 %. The survival rate decreases to 50% with the development of distant metastases. Prostate cancer progresses relatively slowly, with the bone being the most common site of distant metastasis. In addition to morphological evaluation methods, such as

simple radiography, computed tomography (CT), and magnetic resonance imaging (MRI), metabolic evaluation methods, including bone scintigraphy and positron emission tomography/CT (PET/CT), using tracers such as sodium fluoride (NaF), fluorodeoxyglucose (FDG), or prostate-specific membrane antigen (PSMA), have been used. In particular, bone scintigraphy is widely used because of its simplicity in

\*Corresponding author: Kazuto Funakoshi. Department of Radiation Oncology, Saitama Medical University Hospital 38 Morohongo, Moroyama, Iruma-gun, Saitama 350-0495, Japan. Tel: +81-49-276-1111; FAX: +81-49-276-1797; E-mail: kfune@saitama-med.ac.jp

© 2025 mums.ac.ir All rights reserved.

This is an Open Access article distributed under the terms of the Creative Commons Attribution License (<http://creativecommons.org/licenses/by/3.0>), which permits unrestricted use, distribution, and reproduction in any medium, provided the original work is properly cited.

identifying the presence and extent of metastasis and in determining treatment efficacy (1, 2). PET/CT is also considered useful but is less widely used than bone scintigraphy (3). Bone metastases from prostate cancer tend to show osteogenic changes and are easy to detect by bone scintigraphy owing to their increased accumulation (4, 5).

Recently, with the widespread use of semiconductor gamma cameras, short-time bone single-photon emission computed tomography (SPECT) evaluation of bone metastases has been reported (6, 7). Although SPECT or SPECT/CT imaging improves diagnostic performance, the addition of SPECT images increases the total scan time. Patients with bone metastases typically undergo frequent bone scintigraphy; therefore, it is important to minimize radiation exposure and perform examinations in a short time.

Furthermore, long scanning times are often associated with discomfort, particularly for sick patients. Compared to conventional scintillation cameras, semiconductor cameras with cadmium-zinc-telluride (CZT) detectors have high energy and spatial resolution; therefore, they reduce the amount of contrast agent injected and shorten the test time (1) (8, 9).

Clinical evaluation of short-term bone SPECT/CT acquisition with whole-body CZT detectors has been reported (10). Furthermore, the gamma camera of GE Healthcare is equipped with a new feature called SwiftScan that allows data to be collected while the detector is moving. Simulations of human phantoms using CZT cameras have been reported (11, 12), but no clinical applications have yet been reported.

The use of SwiftScan may further reduce collection time; however, the aforementioned study (10) did not examine this function or its quantitative effects. Therefore, this study aimed to evaluate the quality and associated quantitative value of the SwiftScan in short-time bone SPECT using a CZT camera.

## Methods

### Patients

Ten patients with bone metastases from prostate cancer who underwent list-mode SPECT/CT imaging with a whole-body semiconductor camera at our hospital between December 2019 and February 2022 were included. The 130 lesions of 10 patients from the 150 lesions of 13 patients in a previous study (Yamane et al. *Sci Rep*, 11(1): 24320) were evaluated. The number of patients analyzed was 76.9%, and 86.6% of the lesions were analyzed. Because a long acquisition time is usually mandatory in standard SPECT

imaging protocols, we evaluated the data of 10 patients for whom two or more table positions were necessary for SPECT acquisition, which is inconvenient for sick patients.

This retrospective study was approved by the Ethical Review Board of Saitama Medical University Hospital (numbered 2021-138 dated March 4, 2022), and the requirement for written informed consent was waived.

### Bone SPECT/CT imaging

<sup>99m</sup>Tc-methylene diphosphonate (PDR Radio-pharma, Inc. Tokyo, Japan) was injected intravenously and a standard target dose of 740 MBq was administered. The actual injected dose was calculated by measuring the dose in the syringe before and after the injection. After approximately 3 h, the patients were asked to void and images were acquired using a whole-body semiconductor camera (GE Healthcare, Chicago, IL, USA. Discovery NM/CT 670 CZT scanner). Standard-scan SPECT/CT images were acquired using a parallel flat board collimator with a non-circular orbit, wide energy range, and high resolution. Images were collected using a step-and-shoot method that rotated 360° in a noncircular orbit, and 60 locations were collected at 6° each during rotation. Unlike the conventional frame mode, in which the  $\gamma$ -ray counts are accumulated on predetermined position coordinates in memory, the collection was performed in list mode, which records the time, position, and energy of each incident  $\gamma$ -ray, in addition to storing the position information directly from the detector. SwiftScan combines a low-energy high-resolution collimator with the tomography mode. In SPECT acquisition, in addition to the usual step-and-shoot acquisition every 6°, the collection of 3° immediately before and after the rotation was assigned to the collection every 6° before and after the rotation. The energy range was 140 keV  $\pm$  7.5%. The collection time for each table was approximately 10 min. All SPECT images were reconstructed using the ordered subset expectation-maximization (OSEM) approach. The number of iterations was 4, the subset was 10, the matrix size was 128 $\times$ 128, and the voxel size was 4.42 $\times$ 4.42 $\times$ 4.42 mm. The ASiR reconstruction technique (GE Healthcare) was used to obtain CT images. The parameters were 120 keV, auto mA, noise index 35, 512 $\times$ 512 matrix, 1.375 pitch, and 0.5-second rotation. The first 5, 10, 25, 50, 75, and 100% of the images in the list-mode data were reconstructed on a workstation (GE Healthcare. Xeleris ver. 4.1) from 100% images. Three-dimensional maximum intensity projection (3D-MIP) images were generated to determine

the overall image quality. Images were captured with and without the Swift Scan.

**Image quality assessment**

Visual evaluation of the 3D-MIP images was performed by two observers using a 5-point scale with 5, 4, 3, 2, and 1 representing “excellent”, “good”, “fair”, “poor”, and “very poor”, respectively Disagreements between the two observers were resolved by consensus.

**Setting of the region of interest**

The region of interest (ROI) was defined as the area of increased accumulation reflective of bone metastases on standard images. The maximum standardized uptake value (SUV<sub>max</sub>) was measured for each ROI. The reference area was set at the proximal femur, which is away from the metastatic lesion. Two experts in nuclear medicine defined the ROI. The ROI positioning and SUV<sub>max</sub> calculations were performed using a workstation (Xeleris).

**Statistical analysis**

The intraclass correlation coefficients (ICC) of SUV<sub>max</sub> for each reconstructed percentage and

normal examination time, with and without SwiftScan, were examined. In a previous study (10), the ICC value was > 0.8, indicating a near-perfect correlation. To evaluate these differences, a Bland–Altman plot was constructed for each patient and the percentage change in each SUV<sub>max</sub> was calculated. The contrast-to-noise ratio (CNR) was calculated to evaluate image quality using the following formula:

$$CNR = \frac{SUV_{max} \text{ of the lesion} - SUV_{mean} \text{ of the reference}}{\text{standard deviation of the reference SUV}}$$

**Results**

A total of 130 metastatic lesions were analyzed in 10 patients. The doses injected ranged from 662.3 to 878.1 MBq, with a median of 732.8 MBq. The time from injection to the start of testing ranged from 165 to 220 min, with a median time of 200.5 min (Table 1). The obtained SPECT images are shown in Figure 1. Images captured with and without SwiftScan were composed for each period, with 100% of the images captured at the standard time using SwiftScan.

**Table 1.** Patient characteristics

Patient no	Age (years)	Dose (MBq)	SPECT table position number of bed positions	Time between tracer injection SPECT start (min)	No. of measurement number of lesions
1	82	878.1	3	206	21
2	76	739.6	2	194	11
3	69	662.3	2	207	11
4	65	868.9	2	200	21
5	83	687.0	3	204	8
6	72	673.0	2	197	7
7	74	699.0	2	198	10
8	76	764.9	2	220	11
9	74	726.0	2	201	18
10	79	765.1	2	165	12
Median	75	732.8	2	200.5	11

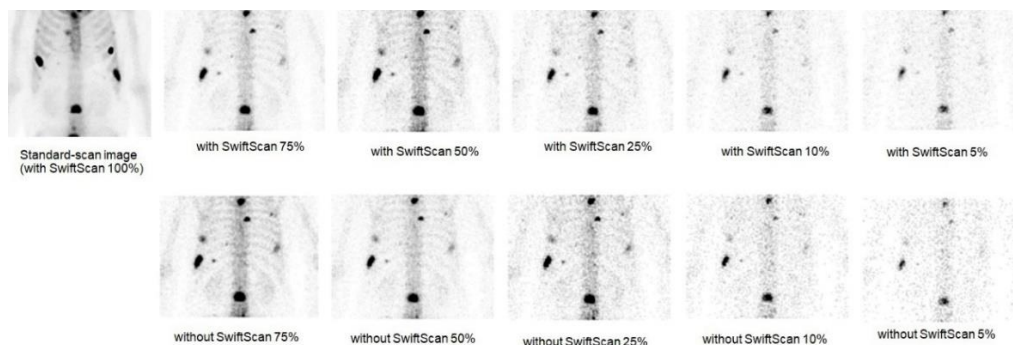


**Figure 1.** Standard-scan image and short-time imaging scan with and without SwiftScan. The images were obtained within a short acquisition time with and without SwiftScan, wherein normal imaging with SwiftScan was used as a reference point (100%)

The results of the image quality assessment of the 3D-MIP images are summarized in Figure 2. On visual assessment, the image quality of the 100% scan with SwiftScan was rated 5 in all 10 patients. The image quality score decreased as a function of imaging time, with and without SwiftScan. However, when an image quality

score of 4 (good) or better was considered clinically acceptable, it was maintained at 4 or better in the scans at 75% and 50% duration images with SwiftScan, whereas only the scans at 75% duration images was considered acceptable without SwiftScan.

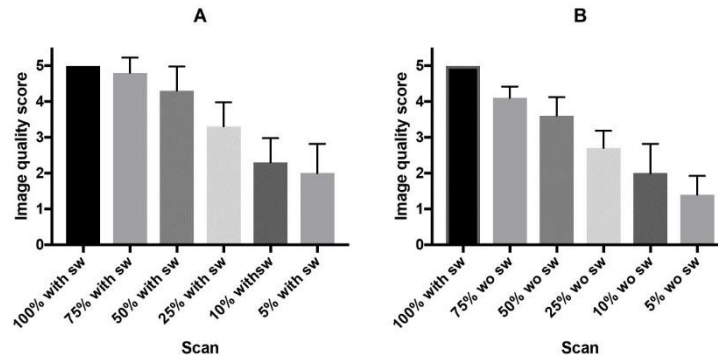


Figure 2. Image quality scores with (A) and without (B) SwiftScan

The ICC value was as high as 0.952, even at 5% relative to the standard time, without SwiftScan, and remained even higher, at 0.990, with SwiftScan (Table 2). The Bland–Altman plots,

with and without SwiftScan, for each acquisition time versus the standard acquisition time are shown (Figures 3 and 4).

Table 2. Intraclass correlation coefficient (ICC)

Against standard acquisition time (With SwiftScan as 100%)	With SwiftScan	Without SwiftScan
100%	-	0.999
75%	0.999	0.998
50%	0.999	0.997
25%	0.997	0.994
10%	0.993	0.982
5%	0.990	0.952

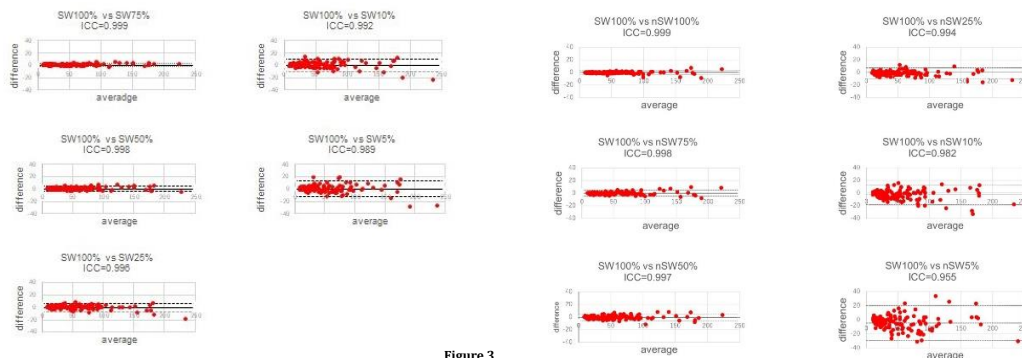


Figure 3

Figure 4

Figures 3, 4. Bland–Altman plots for the images with (Figure 3) and without (Figure 4) SwiftScan

The difference between the measured values of the short-time acquisition images with and without SwiftScan and the respective ICC values, with the reference image with SwiftScan, was set to 100%. The solid lines represent the bias lines and the dashed lines represent the upper and lower confidence intervals

Horizontal dashed lines are 95% confidence intervals  
ICC, Intraclass correlation coefficient

The percentage of  $SUV_{max}$  changes >10% without SwiftScan was 0.7% for full-duration images in the list-mode data, 4.6% at 75%, 16.9% at 50%, 28.5% at 25%, 56.2% at 10%, and 68.4% at 5%-duration images. In contrast (Figure 5), SwiftScan suppressed the rates to 0.75% at 75%, 3.85% at 50%, 20.8% at 25%, 30.8% at 10%, and 40.8% at 5%-duration images.

The percentage change based on full-duration images using SwiftScan is shown in Figure 5. As shown in Figure 6, the  $SUV_{max}$  changes from 0 to 9.5 (median 1.1) at 75%, 0.1 to 11.5 (1.65) at 50%, 0 to 15.7 (2.1) at 25%, 0.1 to 33.2 (4.2) at

10%, 0.2 to 8.9 (5.65) at 5%-duration images without SwiftScan. In contrast, the  $SUV_{max}$  changes in absolute values were from 0 to 5.4 (median 0.8) at 75%, 0 to 6.5 (1.4) at 50%, 0 to 19.1 (1.7) at 25%, 0 to 24.2 (2.8) at 10%, 0 to 29.9 (2.6) at 5%-duration images with SwiftScan. CNR was 95.3 in images captured at 75% of the standard duration, 88.3 at 50%, 69.2 at 25%, 45.7 at 10%, 31.6 at 5%-duration images, and the SwiftScan maintained high values at 96.9, 91.7, 78.0, 71.6, and 62.0 respectively (Table 3). Figure 7 shows the CNR.

CNR did not differ significantly with or without

SwiftScan if the acquisition time was sufficiently long; however, for shorter acquisition times,

CNR was better with SwiftScan than without SwiftScan.

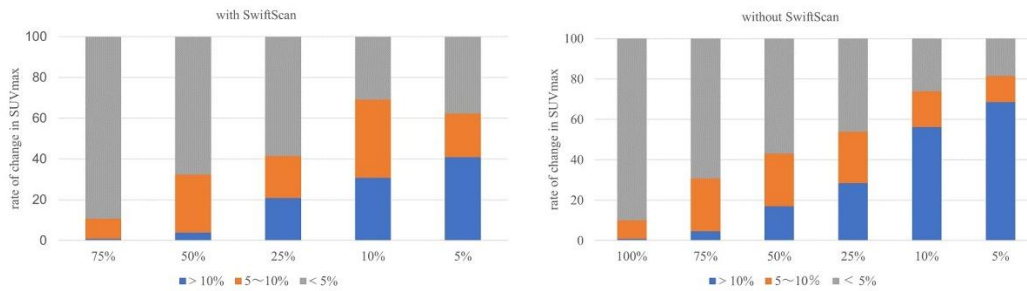


**Figure 5.** Rate of change in  $SUV_{max}$   
 The changes in  $SUV_{max}$  during short-time acquisition with and without SwiftScan are shown. Changes >10% are shown in light blue, changes in the range of 5–10% are shown in orange, and changes < 5% are shown in gray, using the standard test with SwiftScan as 100%  $SUV_{max}$ , maximum standardized uptake value

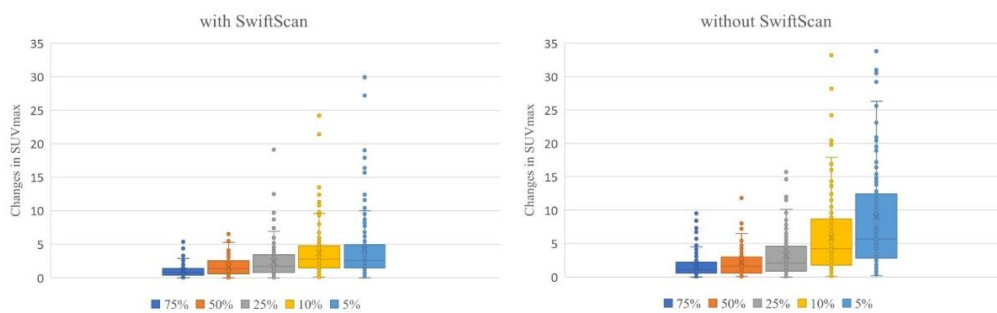


**Figure 6.** Actual changes in  $SUV_{max}$   
 The upper and lower whiskers indicate the 10<sup>th</sup> and 90<sup>th</sup> percentiles of the data, respectively  $SUV_{max}$ , maximum standardized uptake value

**Table 3.** Contrast to Noise Ratio

Against standard acquisition time (With SwiftScan as 100%)	With SwiftScan	Without SwiftScan
100%	-	97.9
75%	96.9	95.3
50%	91.7	88.3
25%	78.0	69.2
10%	71.6	45.2
5%	62.0	31.6

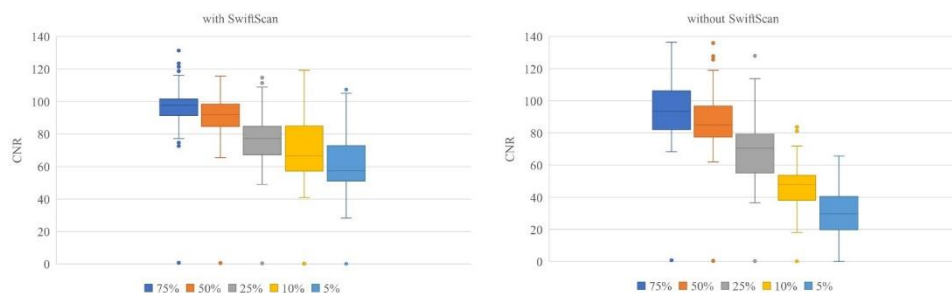


**Figure 7.** A box-and-whisker plots of CNR  
 The box-and-whisker plots of each CNR for short-time acquisition images, with and without SwiftScan, are shown. The upper and lower whiskers indicate the 10<sup>th</sup> and 90<sup>th</sup> percentiles of the data, respectively CNR, Contrast-to-noise ratio

### Discussion

The main results of the study are as follows:  
 1. Visual analysis showed that when an image quality score of 4 (good) or better was considered clinically acceptable, it was maintained at 4 or

better in the 75% and 50%-duration images with SwiftScan, whereas only the 75%-duration images was considered acceptable without SwiftScan.

2. ICC values show no difference with or without



SwiftScan for long-duration examinations, but higher values are obtained with SwiftScan for shorter acquisition times.

3. Although the rate of change in  $SUV_{max}$  increased with a short acquisition time, with or without SwiftScan, the use of SwiftScan reduced the high rate of change.

4. CNR did not differ significantly with or without SwiftScan if the acquisition time was sufficiently long; however, for shorter acquisition times, CNR was better with SwiftScan than without SwiftScan.

The results of the visual assessment of image quality indicate that when the image quality was "good" or better was considered acceptable, the SwiftScan allowed a 50% reduction in acquisition time whereas the acceptable reduction was 25% without SwiftScan. Thus, using SwiftScan was beneficial in reducing the acquisition time in bone SPECT.

The ICC is an indicator used to evaluate reproducibility. These values were high, regardless of the presence or absence of SwiftScan. Considering that values of 0.75 or higher indicate good reproducibility, the values obtained in our study can be considered to have high reproducibility.  $SUV_{max}$  is widely used and reproducible. It can be measured independently of the ROI size (2) and has been used to predict bone metastasis (4). Whereas the CNR showed an increase in background noise with a reduction in acquisition time with and without the SwiftScan, the rate decreased by 10% without the SwiftScan and remained relatively constant up to 5% with the SwiftScan. Short-term images obtained without SwiftScan had inferior image quality, which increased the possibility of false positives. Notably, SwiftScan provides sufficiently good image quality, even with a short scanning time. A short acquisition time is desirable for patients with bone metastases, as it allows the examiner to perform an increased number of examinations. In addition, the number of injected radiopharmaceuticals is reduced, and for patients who are likely to be tested multiple times, this reduces radiation exposure. Although it is possible to collect sufficient data approximately 25% of the time (6), the initial diagnosis encompasses approximately 75% of the total acquisition time, and a short acquisition time may be desirable for follow-up. Normally, one step every 6° required 20 s to complete. This included a collection time of 17 s and a move time of 3 s. Because the collection was performed at 360° with two detectors, one detector required approximately 600 s for 30 steps. The collection time was 510 s, and the movement time was 90 s. As the collection time

at 100% was 510 s, SwiftScan should reduce the collection time by this amount. At 75%, the collection time was 382 s and the travel time was 90 s for a total of 472 s. Similarly, at 50%, 255 s + 90 s for 345 s. At 25%, 127 s + 90 s for a total of 217 s. At 10%, 51 s + 141 s for 191 s. At 5%, the time was shortened to 25 s + 90 s for a total of 117 s. In this study, we found that the addition of 90 s to each scan was substantial.

The ICC values with or without SwiftScan provided sufficient evaluation results with a short acquisition time. However, with shorter collection times, SwiftScan increased reproducibility.

$SUV_{max}$  is associated with a higher rate of change as the acquisition time shortens, but the rate of change decreases when SwiftScan is applied; therefore, SwiftScan should be used for short acquisition time.

The CNR indicates that the noise tends to increase as the acquisition time decreases. Therefore, the shorter the acquisition time, the better the images obtained using SwiftScan.

Currently, there are no firm indicators on SwiftScan, but it can be considered as one of them.

A limitation of this study is that owing to the paucity of cases, a histological examination of patients with prostate cancer bone metastases was not performed. Bone metastases from prostate cancer are predominantly osteogenic lesions, but there is a large proportion of osteolytic lesions as well, and the results may differ for mixed lesions (13). Further research is required to assess whether this approach can be applied to other cancer types.

## Conclusion

With the use of SwiftScan, a 50% reduction in acquisition time was considered acceptable for image quality with reproducible quantitative indices such as  $SUV_{max}$  and CNR.

## Acknowledgements

No potential conflicts of interest were disclosed.

## References

1. Koulikov V, Lerman H, Kesler M, Sapir EE.  $^{99m}Tc$ -MDP bone scintigraphy of the hand: comparing the use of novel cadmium zinc telluride (CZT) and routine NaI(Tl) detectors. *EJNMMI Research*. 2015; (1): 63.
2. Rohani MFM, Nawi NM, Shamim SE, Sohaimi WFW, Zainon WMNW, Musarudin M, et al. Maximum standardized uptake value from quantitative bone single-photon emission computed tomography/computed

- tomography in differentiating metastatic and degenerative joint disease of the spine in prostate cancer patients. *Ann Nuc Med*. 2020; 34(1): 39–48.
3. Tabotta F, Jreige M, Schaefer N, Becce F, Prior JO, Lalonde MN. Quantitative bone SPECT/CT: high specificity for identification of prostate cancer bone metastases. *BMC Musculoskelet Disord*. 2019; 20(1): 619.
  4. Kuji I, Yamane T, Seto A, Yasumizu Y, Shirotake S, Oyama M. Skeletal standardized uptake values obtained by quantitative SPECT/CT as an osteoblastic biomarker for the discrimination of active bone metastasis in prostate cancer. *Eur J Hybrid Imaging*. 2017; 1(1): 2.
  5. Logothetis CJ, Lin SH. Osteoblasts in prostate cancer metastasis to bone. *Nat Rev Cancer*. 2005; 5(1): 21–8.
  6. Picone V, Makris N, Boutevin F, Roy S, Playe M, Soussan M. Clinical validation of time reduction strategy in continuous step-and-shoot mode during SPECT acquisition. *EJNMMI Physics*. 2021; 8(1): 10.
  7. Chikamori T, Hida S, Tanaka N, Igarashi Y, Yamashita J, Shiba C, et al. Diagnostic Performance of a Cadmium-Zinc-Telluride Single-Photon Emission Computed Tomography System With Low-Dose Technetium-99m as Assessed by Fractional Flow Reserve. *Circ J*. 2016; 80(5): 1217–24.
  8. Goshen E, Beilin L, Stern E, Kenig T, Goldkorn R, Haim SB. Feasibility study of a novel general purpose CZT-based digital SPECT camera: initial clinical results. *EJNMMI Phys*, 2018; 5(1): 6.
  9. Yamane T, Kondo A, Takahashi M, Miyazaki Y, Ehara T, Koga K, et al. Ultrafast bone scintigraphy scan for detecting bone metastasis using a CZT whole-body gamma camera. *Eur J Nucl Med Mol Imaging*. 2019; 46(8): 1672–77.
  10. Yamane T, Takahashi M, Matsusaka Y, Fukushima K, Seto A, Kuji I, et al. Satisfied quantitative value can be acquired by short-time bone SPECT/CT using a whole-body cadmium-zinc-telluride gamma camera. *Sci Rep*, 2021; 11(1): 24320.
  11. Shiba T, Sekikawa Y, Tateoka S, Shinohara N, Inoue Y, Kuroiwa Y, et al. Verification of the effect of acquisition time for SwiftScan on quantitative bone single-photon emission computed tomography using an anthropomorphic phantom. *EJNMMI Physics*. 2022; 9(1): 48.
  12. Shibutani T, Onoguchi M, Naoi Y, Yoneyama H, Konishi T, Tatami R, et al. The usefulness of SwiftScan technology for bone scintigraphy using a novel anthropomorphic phantom. *Sci Rep*, 2021; 11(1):2644.
  13. Isoda T, Baba S, Maruoka Y, Kitamura Y, Tahara K, Sasaki M, et al. Influence of the Different Primary Cancers and Different Types of Bone Metastasis on the Lesion-based Artificial Neural Network Value Calculated by a Computer-aided Diagnostic System, BONENAVI, on Bone Scintigraphy Images. *Asia Ocean J Nucl Med Biol*. 2017; 5(1). 49–55.